Task-specific topographical maps of neural activity in the primate lateral prefrontal cortex

Jinkang Derrick Xiang*[1,2], Megan Roussy[2,4], Benjamin Corrigan[2,10], Roberto A. Gulli[2,8], Rogelio Luna[2,9], Maryam Hasanzadeh Mofrad[1,7], Lyle Muller[1,7], Jörn Diedrichsen[1,5,6], Taylor W. Schmitz[1,2,4], Julio Martinez-Trujillo[2,4], Marieke Mur*[1,3,5]

[1]Western Institute for Neuroscience, University of Western Ontario, London, ON, Canada
[2]Robarts Research Institute, University of Western Ontario, London, ON, Canada
[3]Department of Psychology, University of Western Ontario, London, ON, Canada
[4]Department of Physiology and Pharmacology, University of Western Ontario, London, ON, Canada
[5]Department of Computer Science, University of Western Ontario, London, ON, Canada
[6]Department of Statistical and Actuarial Sciences, University of Western Ontario, London, ON, Canada
[7]Department of Mathematics, University of Western Ontario, London, ON, Canada
[8]Zuckerman Mind Brain Behavior Institute, Columbia University, New York, The United States
[9]Facultad de Medicina y Ciencias Biomédicas, Universidad Autónoma de Chihuahua, Chihuahua City, Mexico
[10]Department of Biology, York University, North York, ON, Canada

Abstract

Neurons in the primate lateral prefrontal cortex (LPFC) flexibly adapt their activity to support a wide range of cognitive tasks. Whether and how the topography of LPFC neural activity changes as a function of task is unclear. In the present study, we address this issue by characterizing the functional topography of LPFC neural activity in awake behaving macaques performing three distinct cognitive tasks. We recorded from chronically implanted multi-

*Correspondence: jxiang27@uwo.ca (Jinkang Derrick Xiang), mmur@uwo.ca (Marieke Mur).

electrode arrays and show that the topography of LPFC activity is stable within a task, but adaptive across tasks. The topography of neural activity exhibits a spatial scale compatible with that of cortical columns and prior anatomical tracing work on afferent LPFC inputs. Our findings show that LPFC maps of neural population activity are stable for a specific task, providing robust neural codes that support task specialization. Moreover, the variability in functional topographies across tasks indicates activity landscapes can adapt, providing flexibility to LPFC neural codes.

Keywords: Lateral prefrontal cortex, rhesus macaque, multi-electrode electrophysiology, cognitive flexibility, functional maps, spatial scale, cortical columns

---

1. Introduction

Flexibility is one of the defining properties of higher-order cognitive functions supported by the primate lateral prefrontal cortex (LPFC). Unlike neural populations in primary sensory areas, where activity is dominated by stimulus input, LPFC neurons flexibly adapt their activity according to rules, contextual associations and feedback associated with different tasks, even when stimulus inputs are held constant (Duncan, 2001; Freedman et al., 2001; Miller and Cohen, 2001; Lennert et al., 2011; Lennert and Martinez-Trujillo, 2013). This flexibility is shaped in part by the diversity of connections LPFC neurons receive, which is more heterogeneous than for sensory neurons (Goldman-Rakic, 1988; Fuster, 2015). Because of their diverse connections, response profiles of LPFC neurons often exhibit selectivity to mixtures of task features, e.g., firing maximally only to a specific combination of rule, context and feedback (Rigotti et al., 2013; Fusi et al., 2016).

The selectivity of individual LPFC neurons to different combinations of task features creates unique challenges to understanding their functional organization. In the visual cortex, individual neurons with preferences for similar stimulus features typically assemble into locally connected populations, giving rise

to functional organizations which can be spatially delineated using stimulus mapping techniques (Wandell et al., 2007). For instance, stimulating different visual field locations (Brewer et al., 2002), stimulus orientations (Fang et al., 2022), or object categories (Bell et al., 2009; Bao et al., 2020) reveals maps of neural populations with distinct feature preferences in striate and extrastriate cortex, respectively. The response profiles of these stimulus-tuned populations persist over days, weeks and months (Margolis et al., 2012; McMahon et al., 2014; Cossell et al., 2015), forming stable topographies with a columnar spatial scale (Hubel and Wiesel, 1968; Tanaka, 1996) detectable using recording techniques such as multi-electrode arrays and functional magnetic resonance imaging (fMRI) (Brewer et al., 2002; Yacoub et al., 2008; Bell et al., 2009; Bao et al., 2020). However, it remains an open question whether LPFC exhibits task-specific functional topographies (Markowitz et al., 2015; Masse et al., 2017; Bullock et al., 2017; Leavitt et al., 2018), and if so, whether these topographies are stable over time (Driscoll et al., 2017; Muysers et al., 2024), and have a spatial scale similar to those of other cortical areas. Testing for task-specific topographies of LPFC activity in primates, i.e., 'task mapping', has proven challenging due to constraints on the complexity and diversity of the 'task space' typically sampled in a given experiment (Yang et al., 2019a). Primate electrophysiology studies often probe only a single task, or task features which are not sufficiently distinct from one another, and do not analyze session-to-session variability in neural activity to characterize population stability.

If task-specific functional topographies exist in LPFC at a spatial scale similar to sensory cortical areas, then this functional organization should be detectable when mapping responses to different task features embedded in a sufficiently diverse task space, and, replicable over time. Here we examined this possibility by acquiring multi-electrode array data from the LPFC of two macaques who were each trained on three distinct cognitive tasks (Luna et al., 2019; Roussy et al., 2021; Corrigan et al., 2022). From these rich data, we were able to perform task mapping of neural response preferences over a well parameterized set of different task feature combinations. The monkeys performed the

same set of tasks over test sessions spanning multiple days, allowing us to assess the stability of task-tuned population responses over time.

We show that topographies of LPFC activity are task-specific and stable within a task. We then demonstrate a columnar spatial scale of functional organization, consistent across all three task-specific functional topographies, which recapitulates prior anatomical tracing work examining the afferent input patterns of LPFC from ipsilateral associational cortices and contralateral LPFC (Goldman-Rakic, 1984; Goldman-Rakic and Schwartz, 1982; Leichnetz et al., 1981). Our results indicate that the functional organization of LPFC exhibits stable topographies of task-specific population activity, likely reflecting distinguishable mixtures of afferent sensory and cognitive stimulation.

2. Results

2.1. Topography of LPFC neural activity across time and tasks

The same two rhesus macaque monkeys (monkey B and monkey T) each performed three cognitive tasks (see Figure 1a-c). The first task is an oculomotor delayed response task (ODR) (Luna et al., 2019). The second task is a visuospatial working memory task (VWM) deployed in a virtual-reality environment with naturalistic scenes for stronger attentional engagement (Roussy et al., 2021; Doucet et al., 2016). The third task is a context-dependent decision-making task (CDM), which was also deployed in a virtual-reality environment (Corrigan et al., 2022). Altogether, these three tasks engage a wide spectrum of cognitive functions, including working memory, visuospatial attention, context-dependent decision making and motor planning.

We recorded the responses of neurons in layer II/III of LPFC areas 8A and 9/46, ventral and dorsal to the principal sulcus, using 96-channel multi-electrode Utah arrays (see Supplemental Figure S1). Each array covered a 4 mm $\times$ 4 mm cortical area with 10 $\times$ 10 electrodes ($\sim$0.4 mm spacing). Data were spike sorted and action potential times were extracted and synchronized to task events. To enable spatial mapping of response preferences across the array, we pooled units

measured by the same channel by summing up their spiking activities. We did so after establishing that units measured by the same channel have similar response preferences (see 5.3 for details). The pooled activity reflects the activity of subpopulations of neurons within the area covered by an array channel.

To characterize the spatial organization of prefrontal population codes, we first computed task tuning profiles, one for each channel in each session in each task. Task tuning profiles are vectors that store the firing rates of a channel to the experimental conditions. The time windows for estimating spike rates vary from a few hundred milliseconds up to a few seconds (see 4.4 for details). These time windows were determined based on task structure, monkey behaviour and population decoding results. Next, we computed a channel-by-channel tuning similarity matrix (Figure 1g) for each array in each session in each task. Each element of the matrix represents the Pearson correlation of tuning profiles between a channel pair. The matrix as a whole reflects the similarity of task tuning for all channel pairs, thus capturing the functional topography of task-tuned LPFC activity. For comparative purposes, we also analyzed trial-to-trial fluctuations about the trial averages that define the tuning profiles (see 4.4 for further details). Topographies based on these spontaneous fluctuations, or residuals, are expected to be consistent across tasks (Cole et al., 2014; Kiani et al., 2015). Results of subsequent analyses are consistent across monkeys and arrays.

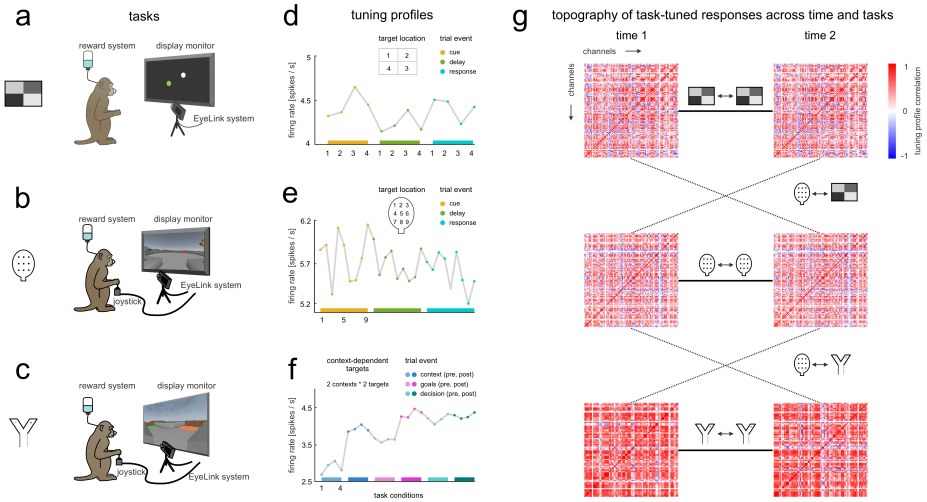

Figure 1: Comparing task-tuned functional topographies in LPFC across time and tasks.

a) Oculomotor delayed response task (ODR). In this task, the monkeys fixated a point on the screen. A cue showed up then disappeared. After a delay, the monkeys saccaded towards the remembered target location.

b) Visuospatial working memory task (VWM). In the cue period, a visual cue showed up in one of nine target locations in a virtual arena, then disappeared. After a delay, the monkeys navigated towards the remembered target location using a joystick.

c) Context-dependent decision-making task (CDM). During the task, the monkeys navigated through an X maze using a joystick. The texture of the corridor walls (wood or steel) indicated the decision context, i.e., which coloured disk the monkey should choose at the bifurcation to get a reward given the texture of the walls (e.g., if wood, choose orange; if steel, choose green).

d) Tuning profile for an example channel in the ODR task. The 16 targets were grouped into 4 quadrants based on their location in the retinotopic reference frame. We computed trial-averaged spike rates for each quadrant during cue, delay and response epochs to estimate the tuning profile for this channel.

e) Tuning profile for the same channel in the VWM task. We computed trial-averaged spike rates for each of the 9 target locations during cue, delay, and response epochs to estimate the tuning profile for this channel.

f) Tuning profile for the same channel in the CDM task. We computed trial-averaged spike rates for each combination of decision contexts and goal configurations in time windows before and after context onset, goals onset, and decision onset to estimate the tuning profile for this channel. Configuration 1: colour associated with wood on the left-hand side; configuration 2: colour associated with wood on the right-hand side.

Figure 1:

g) Schematics for comparing the topography of task-tuned responses across time and tasks. Tuning similarity matrices are shown for 2 example sessions in ODR, VWM and CDM tasks. Elements of the matrices represent the Pearson correlation of tuning profiles between channel pairs. We estimated the consistency of tuning similarity matrices across time within a task (solid horizontal lines) and across tasks (dotted lines) to study how topography of task-tuned responses changes across time and across tasks.

2.2. The topography of LPFC neural activity is stable over time but adaptive across tasks

Examining the tuning similarity matrices, we found that the mean cross-channel correlation (r) over sessions and tasks was 0.50+/-0.21 (mean+/-SD) for monkey B (mB) and 0.43+/-0.17 for monkey T (mT). In the residual similarity matrices, the mean cross-channel correlation (r) over sessions and tasks was 0.08+/-0.04 for mB and 0.14+/-0.08 for mT. To assess whether the functional topography of LPFC neural activity is consistent over time (sessions) and across tasks (ODR, VWM and CDM), we computed the average correlation of the channel-by-channel similarity matrices across sessions within and between tasks (Figure 1g). To control for array shifting across time, we only included sessions spaced apart no more than 20 days for within- as well as between-task comparisons. Given that data for some tasks were acquired more than 20 days apart, between-task comparisons are based on two out of three tasks for each monkey (see 5.2 for further details).

Over time, the consistencies of the task-tuned topographies were as follows: mB: VWM-VWM $r = 0.43$, mB: CDM-CDM $r = 0.25$, mT: VWM-VWM $r = 0.38$ and mT: ODR-ODR $r = 0.21$). In all cases, the r values for within-task consistencies were significantly larger than zero ($p < 0.05$, permutation test, Figure 2a). More importantly, the within-task consistencies for task-tuned topographies were significantly higher than those observed for residual topographies (mB: VWM-VWM $t(54) = 3.97$, $p < 0.001$, mB: CDM-CDM $t(14) = 2.95$, $p = 0.01$, mT: VWM-VWM $t(13) = 3.28$, $p = 0.006$ and mT: ODR-ODR

$t(5) = 2.60$, $p = 0.05$). Hence, over sessions of a given task, the topographies of task-tuned responses are more consistent than the topographies of concurrent trial-to-trial fluctuations in spontaneous activity.

Across different tasks, the consistencies of task-tuned topographies were as follows: mB: VWM-CDM $r = 0.11$, mT: VWM-ODR $r = 0.18$. These consistencies were significantly below their estimated noise ceilings, suggesting that task-tuned functional topographies are not fully consistent across tasks even when considering noise inherent to the data. Moreover, the r values quantifying between-task consistency of task-tuned topographies were either significantly lower than or not significantly different from those observed for residual topographies (mB: VWM-CDM $t(36) = -3.03$, $p = 0.005$, mT: VWM-ODR $t(3) = -0.51$, $p = 0.64$). Hence, between a given pair of two different tasks, the topographies of task-tuned responses are less consistent than the topographies of concurrent spontaneous trial-to-trial fluctuations in activity.

Our analyses suggest that task-tuned functional topographies in LPFC are (1) stable across time within a task: neural populations that have similar tuning on one day tend to have similar tuning on another day, and, (2) adaptive across tasks: neural populations that respond similarly in one task do not necessarily respond similarly in another task.

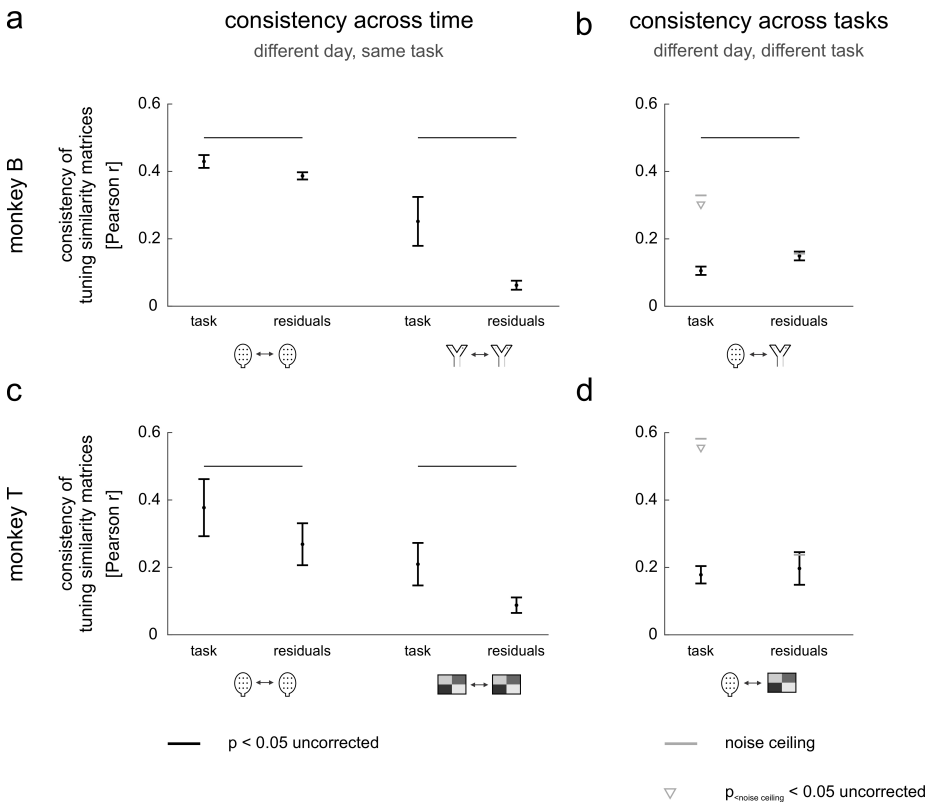

Figure 2: Task-tuned functional topographies in LPFC are stable across time but adaptive across tasks.

a) Consistency of functional topographies across time within a task. The functional topographies are more consistent across time for task-tuned responses than for residuals. Results are shown for the ventral array of monkey B in the VWM and CDM tasks (paired t-test, $p < 0.05$ uncorrected, black horizontal lines indicate significance). Error bars show the standard error of the mean consistency of tuning similarity matrices across session pairs.

b) Consistency of functional topographies between tasks. The functional topographies are less consistent between tasks for task-tuned responses than for residuals. Results are shown for the ventral array of monkey B (paired t-test, $p < 0.05$ uncorrected, the black horizontal line indicates significance). Furthermore, the between-task consistency for task-tuned responses is significantly lower than the noise ceiling (t-test, $p < 0.05$ uncorrected, $\triangledown$ indicates significance), which is not the case for residuals. Grey horizontal line shows the noise ceiling. Error bars show the standard error of the mean consistency of tuning similarity matrices across session pairs.

c, d) as in a, b), but for the ventral array in monkey T, using VWM and ODR tasks.

For both monkeys, the consistencies of functional topographies for task-tuned responses and residuals are significantly higher than chance, both within- and between-tasks (channel permutation test, $p < 0.05$, uncorrected, significance not shown for simplicity).

2.3. Linking the topography of LPFC neural activity to fine-grained spatial maps

Given that feature-tuned neurons are known to cluster in populations at the spatial scale of cortical columns (Hubel and Wiesel, 1968; Tanaka, 1996; Masse et al., 2017), the observed functional patterns of within- and between-task consistency in LPFC (Figure 2) may be expressed spatially by stable clusters of similarly tuned neurons with an adaptive task-dependent 'fingerprint'. To quantify the degree of spatial clustering of channels with similar response preferences on the array, we used the tuning profile as defined in Figure 1d-f, in accordance with previous studies (Leavitt et al., 2018; Bullock et al., 2017; Arbuckle et al., 2020; King et al., 2019). From these tuning profiles, we then computed a spatial autocorrelation function (ACF). A positive autocorrelation indicates that channels spaced at a specified spatial distance have similar tuning profiles, while a negative autocorrelation indicates that channels spaced at the specified distance have dissimilar tuning profiles. Zero indicates no spatial autocorrelation. We systematically varied the spatial distances and plotted the spatial autocorrelation as a function of distance. At a distance of zero, the ACF was set to 1 by definition. We then fitted a Laplacian function to the spatial ACF for each array in each session in each task to capture the exponential decay of the ACF as a function of distance and to quantify the spatial scale of the functional organization. The spatial scale is estimated by the full-width-at-half-maximum (FWHM) of the Laplacian function, which is the FWHM of the 2-dimensional kernel needed to smooth spatially independent tuning profiles to yield the same degree of clustering we see in the data (Diedrichsen et al., 2011).

From the ACFs of both monkeys, we observed a positive autocorrelation up to a distance of 1-2 mm across tasks (Figure 3a). The median of the FWHMs across sessions and tasks is 341 +/- 105 microns (SD), suggesting the existence of fine-grained clusters on the arrays.

To get an impression of the spatial structure of the tuning similarity on the arrays, we next visualized the data using 2-dimensional (2D) multidimensional scaling (MDS). We converted the tuning profile correlations to correlation distances, and applied 2D MDS. Channels were colour-coded based on their lo-

cation in the 2D MDS space and projected back to the arrays (Figure 3b). The MDS array maps confirm that the functional organization in LPFC is stable across time within a task, as can be seen by the similarity between intra-task array pairs in Figure3c. In contrast, LPFC functional organization is adaptive across tasks, as evidenced by the dissimilarity of inter-task array pairs in Figure 3c.

From the 2D MDS array maps, we also observed fine-grained spatial patterns consistent with clustering of population activity according to distinct task-tuned feature preferences. To explore whether these clusters become more pronounced when smoothed according to the empirically derived cluster sizes from the fitted Laplacians, we smoothed the 2D MDS maps using 2D Gaussian kernels whose FWHM matches that of the fitted Laplacians. In all three tasks, smoothing the 2D MDS with its corresponding FWHM kernel revealed clusters of task-tuned population activity similar to maps observed in other cortical areas (Figure 3d) (Brewer et al., 2002; Fang et al., 2022; Yacoub et al., 2008).

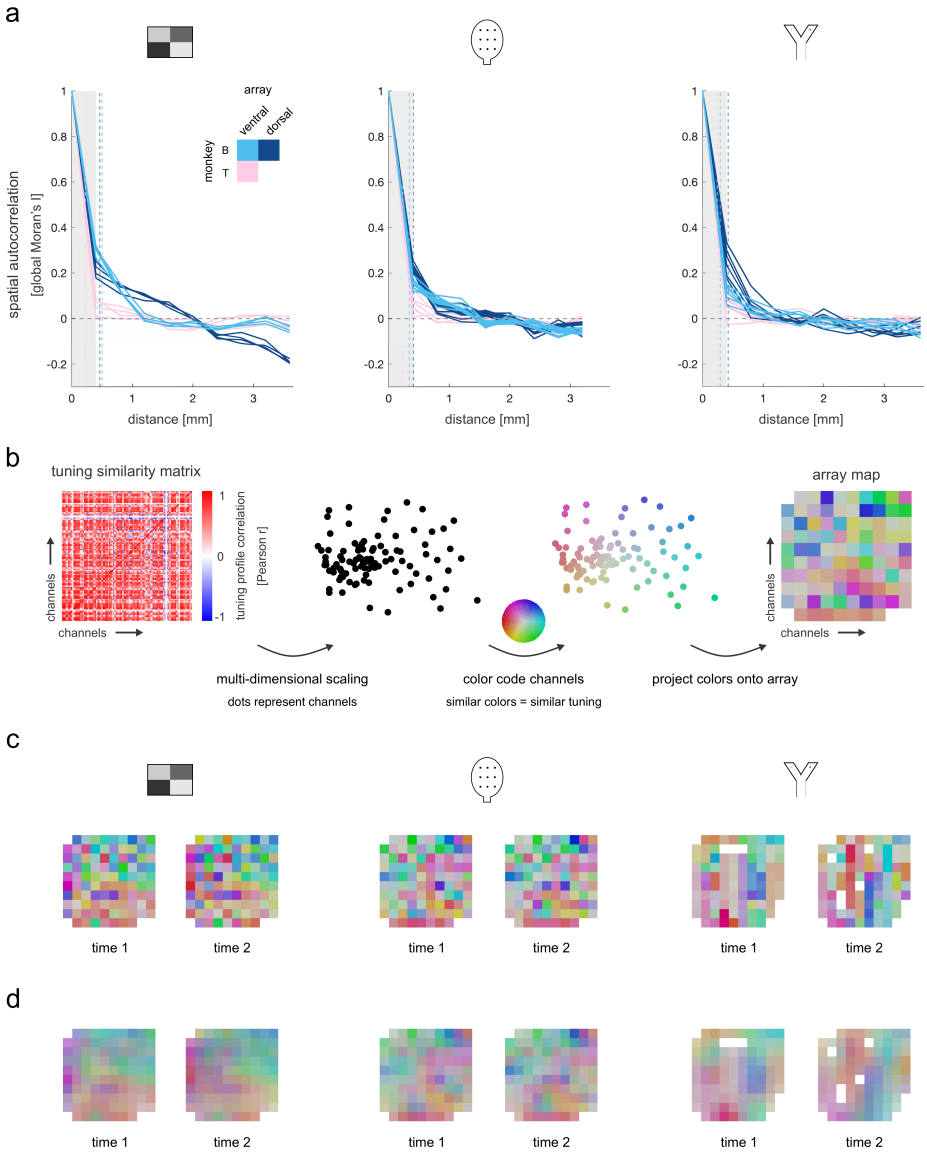

Figure 3: Task-tuned functional topographies in LPFC are organized at a fine-grained spatial scale.

a) Spatial autocorrelation functions (ACFs) for ODR, VWM, and CDM tasks. Solid lines represent the ACFs for individual sessions in each task. Colours reflect the corresponding arrays: light blue for monkey B ventral array, dark blue for monkey B dorsal array, and pink for monkey T ventral array. Grey shaded areas show the width between two immediately neighbouring channels (0.4 mm). Vertical dashed lines show the median full-width-at-half-maximum (FWHM) of fitted Laplacian function across sessions.

Figure 3:

b) Steps taken to visualize channel task-tuning profile similarity on the array. Channels with similar task-tuning profiles are colour-coded similarly.

c) MDS visualizations for monkey B dorsal array in all three tasks, two example measurement sessions per task.

d) Array maps in c) after smoothing with 2D Gaussian kernels whose FWHMs match the fitted Laplacian functions.

Our findings suggest that task-tuned LPFC responses are clustered at the spatial scale of cortical columns. Prior anatomical tracing work on macaque LPFC suggests that cortical columns in the principal sulcus have a width of 300 - 700 microns (Goldman-Rakic, 1984; Goldman and Nauta, 1977; Bugbee and Goldman-Rakic, 1983). We next asked what properties of cortical organization might shape this spatial scale. One possibility is that the afferent input projections from different regions of the brain may exhibit a spatial scale of clustering in the LPFC similar to that of the functional topographies observed in the present work. This would suggest that the structural organization of long-range inputs into LPFC shapes the functional topographies of its task-tuned responses. To test this hypothesis, we acquired a structural connectivity map representing the profile of afferent inputs to the macaque principal sulcus of the LPFC from the contralateral principal sulcus through colossal fibres (i.e., the black stripes), and from the ipsilateral parietal cortex through associational fibres (i.e., the gaps interdigitated with the black stripes) (Goldman-Rakic, 1984). The structural map overlaps the cortical patch measured with multielectrode arrays in the current study (Figure 4a). Because the connectivity map provided coverage of a cortical patch which was larger than the 4 mm $\times$ 4 mm patch covered by the electrode array in the current study, we used a 4 mm $\times$ 4 mm window to randomly sample 210 locations, thereby providing an unbiased estimate of the map's intrinsic spatial frequency (Figure 4b). At each sample, we down-sampled the map to 10 $\times$ 10 pixels (matching the spatial resolution of the array) and computed the spatial ACF using the same strategy as de-

picted in Figure 3a. From these 210 samples, we observed that the mean ACF of the afferent inputs into LPFC closely approximates that observed from the functionally derived topographies in Figure 3a (Figure 4d).

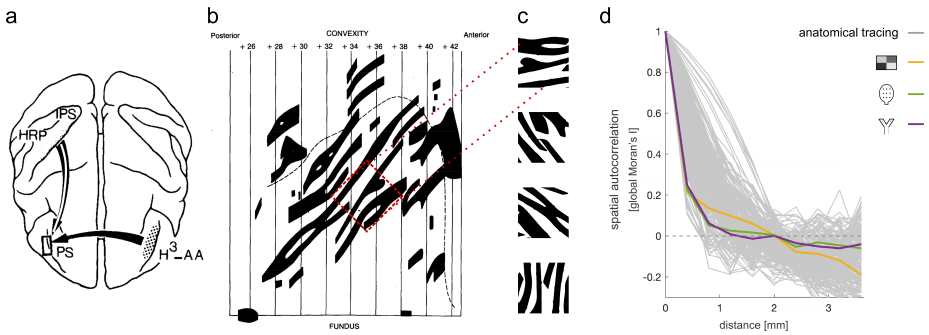

Figure 4: Linking task-specific functional topographies in LPFC to fine-grained structural maps.

a) Anatomical tracing of white matter fibre inputs to macaque LPFC, adapted from (Goldman-Rakic, 1984). LPFC receives inputs through contralateral colossal fibres of the principal sulcus (PS; indicated by the solid black arrow) and ipsilateral association fibres from the intraparietal sulcus (IPS; indicated by the white strike arrow), providing the neural basis for interhemispheric integration. HRP = horeradish peroxidase, $H^3 - AA$ = tridared amino acids.

b) Topographical input patterns of LPFC, adapted from (Goldman-Rakic, 1984). The black dashed line represents the rim of the principal sulcus. The black stripes show the reconstructed terminal fields of colossal fibres in the principal sulcus, reflecting inputs from the contralateral principal sulcus. The square in red shows an example of the total 210 sampled cortical patches. In a separate experiment, interdigitated white areas were shown to receive inputs from IPS.

c) Examples of randomly sampled cortical patches from the reconstructed map in panel b). Each sample has a coverage of 4 mm $\times$ 4 mm.

d) Grey lines represent the ACFs for each of the 210 randomly sample cortical patches. The yellow, green and purple lines show the mean ACFs of task tuning across sessions for the ODR, VWM and CDM tasks, respectively, for the dorsal array in monkey B.

3. Discussion

We characterized the functional topography, temporal stability, and spatial scale of task-tuned LPFC neural activity by analyzing array recordings from awake behaving macaques performing a range of cognitive tasks (Luna et al.,

2019; Roussy et al., 2021; Corrigan et al., 2022). We show that the spatial topography of task-tuned LPFC neural activity is stable across time within a task but adaptive across tasks. The stability for task-tuned responses is higher than for concurrent spontaneous fluctuations, indicating that the correlation structure among LPFC neural populations is strengthened by task. We further demonstrate that although all three tasks exhibit distinct topographies of task-tuned activity, they converge on a common spatial scale compatible with that of cortical columns. Finally, we show that this spatial scale is likely shaped, in part, by the organization of afferent long-range inputs into the LPFC from distinct cortical areas throughout the brain.

Progress on understanding the functional organization of primate LPFC has been hampered by (1) the limited number of tasks sampled in typical monkey electrophysiology or human functional magnetic resonance imaging (fMRI) studies (Harel et al., 2014; Bullock et al., 2017; Leavitt et al., 2018; Yang et al., 2019a) and (2) a disconnect between the study of structural and functional organization in LPFC (Goldman-Rakic, 1984; Xu et al., 2022; Kiani et al., 2015; Bullock et al., 2017; Leavitt et al., 2018). Below we discuss these obstacles in relation to the current study.

Across the three different tasks examined in this study, we noted that the between-task consistency of LPFC topographies was lower for task-tuned responses than for concurrent spontaneous fluctuations in neural activity, but still shared a significant portion of task-related variance. This shared variance may be driven by similarity in cognitive demands across tasks, which at present is difficult to define objectively. Future studies may benefit from generating 'task ontologies' sampled from a high-dimensional space consisting of diverse but carefully parameterized task features. These task ontologies could then be used to systematically vary the functional structure of the tested task space, e.g., similarity of two distinct tasks to one another or their additivity, thereby enabling exploration of more computationally principled hypotheses about LPFC function, including biased competition (Desimone and Duncan, 1995; Schmitz and Duncan, 2018) and compositional coding (Duncan et al., 2017; Yang et al.,

2019b).

Our findings suggest that LPFC functional topographies are likely shaped by the unique profiles of long-range afferent input (Goldman-Rakic, 1988; Xu et al., 2022), which yield preferences for distinct combinations of task features, i.e., task tuning. The structural organization of a diverse repertoire of long-range synaptic inputs into the LPFC (Goldman-Rakic, 1984) may therefore provide the scaffolding for LPFC's functional organization, by shaping the intrinsic network structure that task activation flows on (Cole et al., 2016; Xu et al., 2022). Future investigations examining fine-grained maps of LPFC task-tuning may necessitate multimodal measures of both LPFC functional and structural organization within the same animals. Several recent studies have laid the groundwork for this critical line of inquiry using innovative techniques integrating functional MRI with LPFC micro-stimulation (Xu et al., 2022) and diffusion MRI (Xu et al., 2020). Finally, our findings in macaques indicate that LPFC functional topographies have a spatial scale that is accessible in humans with high-field fMRI. Looking ahead, cross-species translational work leveraging macaque electrophysiology and human fMRI to map fine-grained task information from LPFC population activity is within reach.

4. Methods

4.1. Subjects and ethics statement

We recorded LPFC neural activity in two male rhesus macaques (*Macaca mulatta*, monkey B and monkey T, 10 and 9 years old) while they were performing three different cognitive tasks across multiple measurement sessions. All training, surgery, and recording procedures conformed to the Canadian Council on Animal Care guidelines and were approved by The University of Western Ontario Animal Care Committee.

4.2. Behavioural tasks

4.2.1. Oculomotor delayed response (ODR) task

Figure 1a illustrates the experimental setup of the oculomotor delayed response task. Each trial began with the appearance of a fixation point at one of 16 predefined locations on a computer screen. Then a target was presented for 1000 ms before it disappeared. The monkeys were asked to maintain fixation for a variable length delay period (1400 ms - 2500 ms, median = 1800 ms) and upon extinction of the fixation point, make a saccade towards the remembered target location to get a reward. More information on the ODR task can be found in (Luna et al., 2019).

4.2.2. Visuospatial working memory (VWM) task

Figure 1b illustrates the experimental setup of the visuospatial working memory task, which took place in a virtual reality environment. Within the virtual arena in the environment, targets were arranged in a 3×3 grid. The time needed to navigate between adjacent targets was $\sim$0.5 s. During the cue period, a visual cue (red rectangle) was presented in one of the nine target locations for 3 seconds, then disappeared. After a 2-second delay, the monkeys navigated towards the remembered target location at a constant speed using a joystick. Upon reaching the correct target, the monkeys received a reward. More information on the VWM task can be found in (Roussy et al., 2021).

4.2.3. Context-dependent decision making (CDM) task

Figure 1c illustrates the experimental setup of the context-dependent decision making task, which was also deployed in a virtual reality environment. The task took place in a double ended Y maze, also termed "X maze" as in (Doucet et al., 2016; Gulli et al., 2020). The monkeys navigated through the X maze using a joystick. The texture of the walls, being brown "wood" or dark grey "steel", indicated which coloured disk the monkeys should choose at the bifurcation to get a reward. In other words, the decision context was specified

by the texture of the walls. We will refer to the coloured disks as goals in subsequent text. More information on the CDM task can be found in (Corrigan et al., 2022).

4.3. Neural recordings

Two 96-channel Utah arrays (4 mm × 4 mm coverage, 10 × 10 electrodes, spaced at 0.4 mm, 1.5 mm in length) (Blackrock Microsystems) were chronically implanted in the left LPFC in each animal. They were located anterior to the arcuate sulcus and on the ventral and dorsal side of the posterior end of the principal sulcus, targeting layers II/III of cortical areas 8A and 9/46. See 5.1 for further details on array placement.

Neural data were recorded using a Cerebus Neural Signal Processor (Blackrock Microsystems). The neural signal was digitized (16 bit) at a sampling rate of 30 kHz. Offline sorting was done with the Plexon Offline sorter (version 4.5.0, Plexon Inc.). Spike sorting for the ODR task was carried out by RL, for the VWM task by MR, and for the CDM task by BWC.

Both monkeys performed multiple sessions for each task. Sessions were acquired on separate days. Monkey B performed 4 sessions for the ODR task, 11 sessions for the VWM task, and 6 sessions for the CDM task. Monkey T performed 4 sessions for the ODR task, 8 sessions for the VWM task, and 9 sessions for the CDM task. One session was excluded from analysis in the VWM task for monkey T due to low trial numbers across experimental conditions. See 5.2 for further details on the measurement sessions. For all tasks, eye positions were monitored using SR Research EyeLink 1000, at a sampling rate of 500 Hz.

The dorsal array in monkey T was excluded from analysis due to low signal-to-noise ratio of recordings at the time of the experimental sessions, which makes it difficult to map the topography of the array.

4.4. Neural data analysis

4.4.1. Computing task tuning profiles

To enable spatial mapping of response preferences across the array, we pooled units recorded from the same channel by summing up their spiking activities. We did so after establishing that units recorded from the same channel have similar response preferences (see 5.3 for details). The pooled activity reflects the activity of subpopulations of neurons within the area covered by an array channel. This area has an estimated diameter of 300 microns based on the impedance of the electrodes.

For each channel in each session in each task, we first computed trial-specific spike rates for each experimental condition and applied a square root transformation to the spike rates to account for the Poisson-like increase of variability with increasing mean firing rates (Yu et al., 2009; Arbuckle et al., 2020). We next computed trial-averaged spike rates by averaging across trials of the same experimental condition, which yielded a task tuning profile for each channel.

More specifically, in the ODR task, the tuning profile for a channel was defined as the trial-averaged spike rates for the 4 quadrants (16 targets were grouped into 4 quadrants based on their location in the retinotopic reference frame, labelled 1-4 starting from bottom left, clockwise) during cue (1000 ms), delay (1400 ms - 2500 ms, median = 1800 ms), and response (first 500 ms) epochs. In the VWM task, the tuning profile for a channel was defined as the trial-averaged spike rates for the 9 target locations during cue (3000 ms), delay (2000 ms), and response (first 500 ms) epochs. In the CDM task, the tuning profile for a channel was defined as the trial-averaged spike rates for the combinations of decision contexts and goal configurations in time windows before and after context onset (50 ms before, 600 ms after), goals onset (500 ms before, 300 ms after), and decision onset (500 ms before, 500 ms after). Goal configuration refers to the location of the disk colour that is associated with wood. If the colour associated with wood is on the left-hand side at the bifurcation, the trial is in configuration 1, otherwise configuration 2.

We then subtracted out the mean firing rate across all experimental conditions. The mean-centred tuning profile reflects the modulation in firing rate by the experimental conditions, providing a rich characterization of channel tuning in each task. The time windows used for computing tuning profiles were based on trial structure, monkey behaviour, and neural population decoding results. Results of subsequent analyses do not critically depend on the exact time windows used.

4.4.2. Computing the topography of task-tuned activity

For each array in each session in each task, we computed a channel-by-channel tuning similarity matrix. Elements in this matrix reflect the Pearson correlation of tuning profiles between channel pairs. The matrix reflects the similarity of task tuning for all channel pairs, thus capturing the similarity structure of tuning across the array. As such, it provides the basis for mapping of tuning similarity across the cortical sheet. This approach can be used to study functional topography (Kiani et al., 2015; Ito and Murray, 2023). Importantly, the tuning similarity matrices abstract from the specific experimental conditions used in a single task, which enables comparison of functional topographies between tasks.

4.4.3. Computing the topography of spontaneous activity

For comparative purposes, we also analyzed trial-to-trial fluctuations about the trial averages that define the tuning profiles. Topographies based on these spontaneous fluctuations are expected to be consistent across tasks (Kiani et al., 2015; Cole et al., 2014). We partitioned the measured spiking activity in two components: task-tuned activity and spontaneous activity or residuals. For each channel in each session in each task, we computed task-tuned activity by replacing the firing rate of each trial with the mean firing rate across trials of the same experimental condition. This corresponds to a tuning profile where the trial-averaged spike rate for each condition is repeated as many times as the number of trials for that condition. We computed residuals by subtract-

ing out the task-tuned activity from the measured spiking activity. We then computed topographies for task-tuned activity and residuals as described in the previous section, but replaced tuning profiles by task-tuned or residual activity vectors. Results reported in Figure 2 are based on the task-tuned and residual topographies, allowing for a direct comparison between the two.

4.4.4. Assessing the consistency of functional topographies across time and across tasks

To assess whether the functional topographies are consistent across time and across tasks, we computed the Pearson correlation of tuning similarity matrices across session pairs within and between tasks (see Figure 1g). Because the matrices are symmetric, we computed correlation coefficients using the upper triangular vector of the matrix. The consistency of functional topographies within and between tasks was estimated as the mean across session pairs. To control for array shifting across time, we only included sessions spaced apart no more than 20 days for within- as well as between-task comparisons. Given that data for some tasks were acquired more than 20 days apart, between-task comparisons are based on two out of three tasks for each monkey (see 5.2 for further details).

To determine whether the estimated consistencies are significantly higher than chance, we permuted channel locations on the array to simulate the null hypothesis of no consistent spatial organization. We performed 1,000 permutations, each yielding an estimate of our test statistic under the null hypothesis. If the actual consistency fell within the top 5 percent of the simulated null distribution, we rejected the null hypothesis of no consistent spatial organization. For between-task consistencies, we did not only test if they were higher than expected for no consistent spatial organization, we also tested if they were lower than expected for a fully consistent spatial organization. We did so by estimating a noise ceiling for between-task consistencies. For each task pair, the noise ceiling is defined as the geometric mean of the within-task consistencies, which reflects the maximum expected between-task consistency given the noise

in the data (Vul et al., 2009). When estimating the noise ceiling, within-task consistencies are based on sessions that are also involved in between-task comparisons. We compared the observed between-task consistencies against the noise ceiling using a one-sided one-sample t-test across session pairs. We compared consistencies of task-tuned and residual topographies using a two-sided paired-samples t-test across session pairs.

4.4.5. Assessing the spatial scale of functional topographies

To assess the spatial scale of the functional topographies, we computed spatial autocorrelation functions (ACFs) of channel tuning profiles on the array. We used global Moran's I as a measure of spatial autocorrelation (Moran, 1950), which is defined as:

$$I = \frac{N}{\sum_i \sum_j w_{ij}} \frac{\sum_i \sum_j w_{ij}(X_i - \bar{X})'(X_j - \bar{X})}{\sum_i (X_i - \bar{X})'(X_i - \bar{X})}$$

where N is the total number of channels on the array; X_i is the mean-centred tuning profile for the ith channel; X_j is the mean-centred tuning profile for the jth channel; $\bar{X}$ is the mean-centred tuning profile averaged across all channels; and w_{ij} is either 1 or 0 (if channel i and channel j are spaced within a specified spatial range, w_{ij} equals 1; otherwise 0).

The numerator estimates the covariances of tuning profiles between channel pairs spaced at a certain distance. The denominator estimates the variances of tuning profiles across all the channels on the array. To account for the fact that some channels appear more frequently than others in the covariance estimates, the variance can be estimated using the following formula as in (King et al., 2019):

$$\frac{\sqrt{\sum_i \sum_j w_{ij}(X_i - \bar{X})'(X_i - \bar{X}) \sum_i \sum_j w_{ij}(X_j - \bar{X})'(X_j - \bar{X})}}{\sum_i \sum_j w_{ij}}$$

Using this formula for estimating the variance ensures that I is bounded between -1 and 1. A positive I indicates that channels spaced at the given

distance have similar tuning profiles; a negative I indicates that channels spaced at the given distance have dissimilar tuning profiles.

To compute spatial ACFs, we systematically varied the spatial distance between channels, from including only immediately neighbouring channels ($0 <$ distance ≤ 0.4 mm) to channels that are spaced apart more than one channel width but no more than two (0.4 mm $<$ distance ≤ 0.8 mm), continuing these steps up and till nine channel widths (3.2 mm $<$ distance ≤ 3.6 mm), and computed the spatial autocorrelation for each distance. At distance 0, the spatial autocorrelation is set to 1 by definition. We computed an ACF for each array in each session in each task.

To quantify the spatial scale of the functional topographies, we fitted a Laplacian function to the spatial ACFs. The Laplacian function captures the exponential decay of channel tuning similarity as the distance between channels increases. The Laplacian function used is defined as follows:

$$f(d) = 1.02 \times e^{-\frac{d}{s}} - 0.02$$

where $d \geq 0$ reflects the distances; and s is a fitted value, reflecting the smoothness of the curve. The full-width-at-half-maximum (FWHM) of the Laplacian curve can be computed using s via the following formula:

$$FWHM = 2 \times s \times \ln(2)$$

The FWHM of a fitted Laplacian function is equivalent to the FWHM of the 2-dimensional kernel required to smooth an array whose channel tuning profiles are spatially independent, to yield the degree of spatial autocorrelation we observe in the data (Diedrichsen et al., 2011). We therefore use the FWHM as an estimator of spatial scale.

4.4.6. Mapping tuning similarity on the array

To visualize the spatial structure of tuning similarity on the arrays, we converted the correlations in the tuning similarity matrix to correlation distances,

and applied 2D multidimensional scaling (MDS) to the distances. Channels were colour-coded based on their location in the 2D MDS space and projected back to the arrays. In the colour space, hue reflects polar angle, and saturation reflects eccentricity. Similar colours indicate similar tuning profiles. As a check, we computed the variance explained in the high-dimensional distances by the low-dimensional distances for a range of MDS dimensions (1-10). We computed the variance explained by first correlating the correlation distances between points (channels) in the original high-dimensional space with the Euclidean distances between points in the low-dimensional MDS space, and then squaring the correlation coefficients (Kiani et al., 2015). The 2D MDS space explains around 80% of the variance in the original high-dimensional space across monkeys, arrays, and tasks.

4.4.7. Linking the functional topographies to structural maps

To relate the spatial scale of the observed functional topographies to prior anatomical tracing work, we repeated the spatial autocorrelation analysis on a reconstructed structural map of afferent input to macaque LPFC (Goldman-Rakic, 1984). This structural map shows the terminal field distributions of callosal fibers projecting from the principal sulcus in one hemisphere to the principal sulcus in the other hemisphere (Goldman and Nauta, 1977). The fibers terminate in a stripe-like pattern, reflecting interdigitation of the contralateral callosal fibers with associational fibers from the ipsilateral parietal cortex (Goldman-Rakic and Schwartz, 1982). The structural map suggests the existence of cortical columns in LPFC, which have been reported to have a width of 300 to 700 microns (Goldman-Rakic, 1984; Goldman and Nauta, 1977; Leichnetz et al., 1981; Goldman-Rakic and Schwartz, 1982; Bugbee and Goldman-Rakic, 1983). To assess the spatial scale of the structural map, we randomly sampled 210 cortical patches with 4×4 mm^2 coverage from the map, simulating array placements. Sampled cortical patches were downsampled to 10×10 to match the measurement resolution of the Utah arrays used in our study. We assessed the spatial ACF for each sampled patch and plotted the distribution

of ACFs across samples. We then examined whether the ACFs observed for the task-tuned topographies fall within the distribution derived from the anatomical tracing map (see Figure 4).

5. Supplementary materials

5.1. Array placements

Figure S1 shows approximate locations of the Utah arrays in each animal.

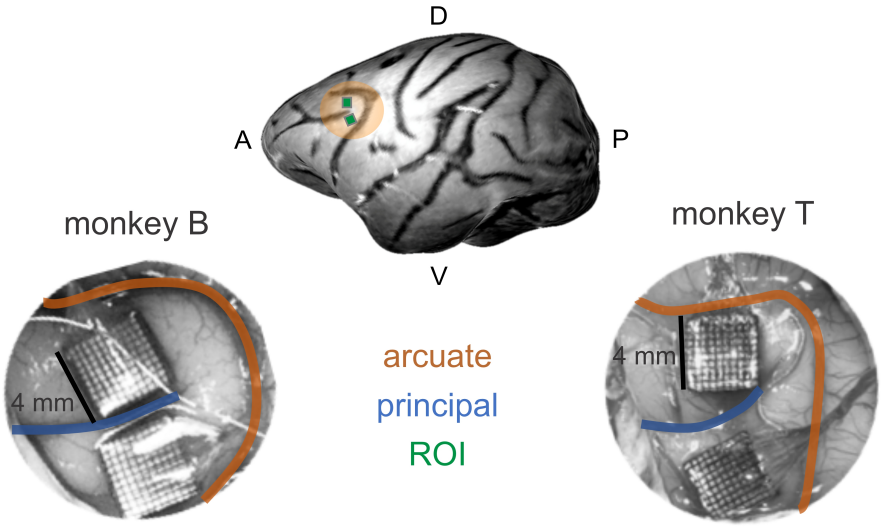

Figure S1: Approximate locations of the Utah arrays. Each monkey had two arrays implanted at the ventral and dorsal end of the principal sulcus in their left LPFC, targeting areas 8A and 9/46.

5.2. Measurement sessions

Data for the three behavioural tasks were acquired sequentially in the following order for both monkeys: CDM, VWM and ODR. Figure S2 shows when each measurement session was acquired over the course of the experiments.

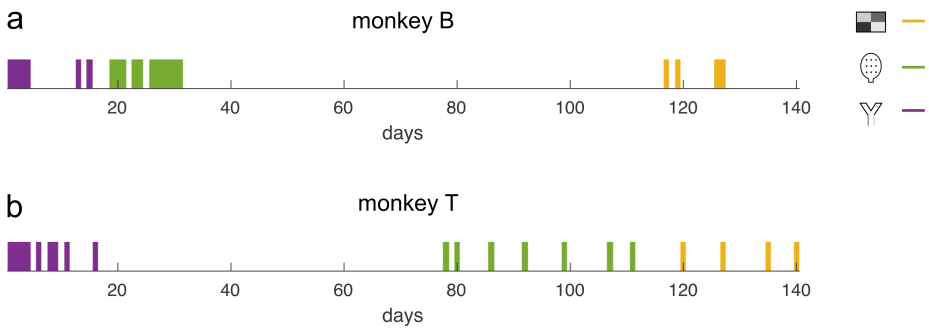

Figure S2: Measurement sessions for each monkey.

a) Relative timing of measurement sessions (days) for monkey B. Yellow bars show sessions for the ODR task, green for the VWM task and purple for the CDM task.

b) As in a), but for monkey T.

5.3. Tuning similarity of units measured by the same channel

To decide whether we can pool spiking activity across units within a channel, we estimated the distribution of tuning profile correlations among units measured by the same channel.

We first estimated mean-centred tuning profiles for each unit in each session in each task, in the same way as described in Figure 1a-c. We then computed tuning profile correlations for all unit pairs within a channel, and averaged correlations across unit pairs for each channel. Figure S3 shows histograms of the averaged correlations across all sessions within a task, for each monkey and array. For completeness, we also show histograms of the number of units measured by individual channels.

Figure S3 shows that the majority of channels measure only one unit. When a channel is measuring from multiple units, the units tend to have similar tuning profiles. Therefore, the spiking activity at the channel level is reasonably representative of units measured, and we performed subsequent analyses at the level of channels.

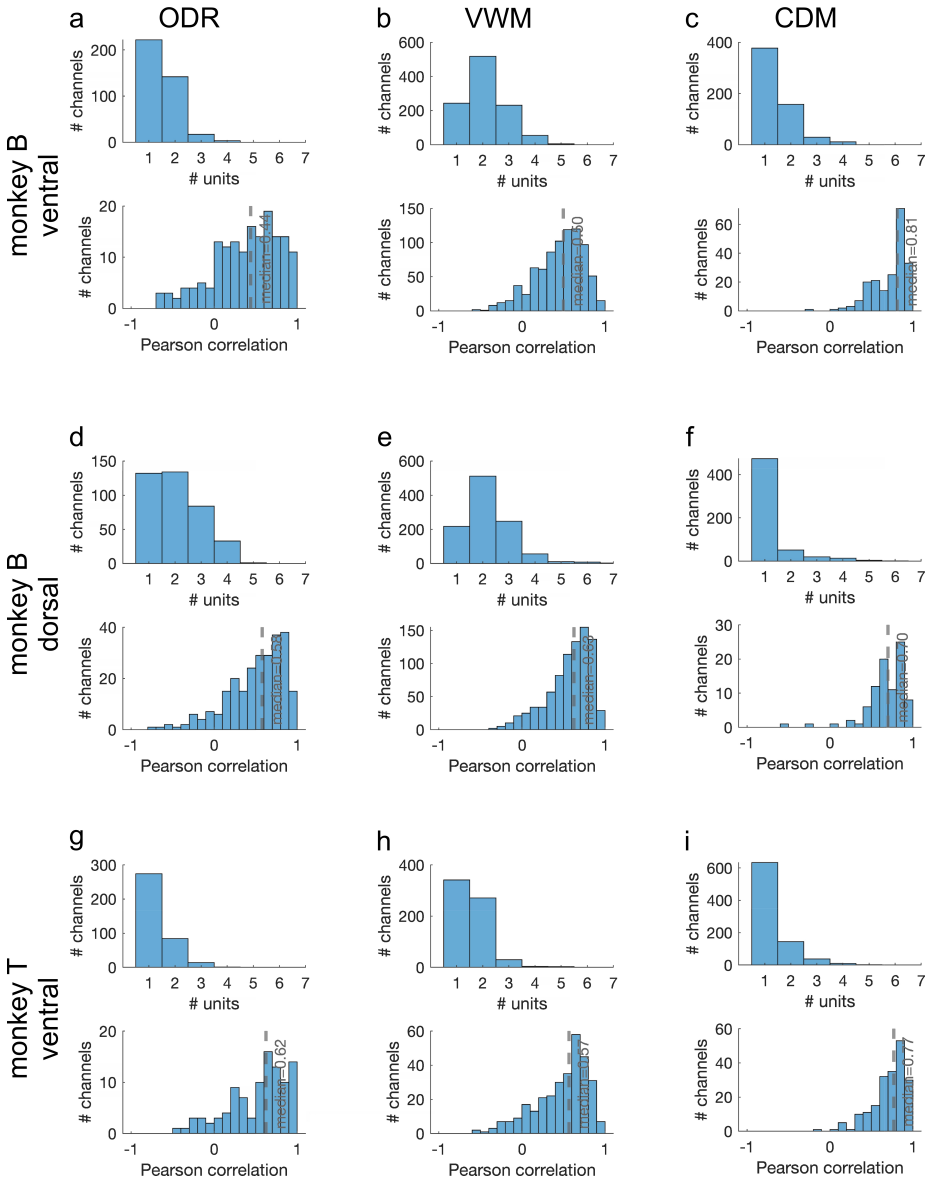

Figure S3: Similarity of tuning profiles across units measured by the same channel.

Figure S3:

a) The consistency of tuning profiles of units within the same channel in monkey B for the ventral array in the ODR task. Upper panel: histogram of the number of units measured by individual channels on the array. Lower panel: histogram of tuning profile correlations between units measured by the same channel. The grey dashed line shows the median.

b) The same as in a) but in VWM task.

c) The same as in b) but in CDM task.

d-f) The same as in a-c), but for monkey B dorsal array.

g-i) The same as in a-c), but for monkey T ventral array.

6. Acknowledgements

This work was supported by the Natural Sciences and Engineering Research Council of Canada (NSERC), the Canadian Institutes of Health Research (CIHR), Neuronex (ref. FL6GV84CKN57) grants, Ontario Graduate Scholarship, Jonathan & Joshua Memorial Graduate Scholarship in Mental Health Research, Mitacs Globalink Graduate Fellowship and McGill David G. Guthrie Fellowship. This work was further supported by BrainsCAN at the University of Western Ontario through the Canada First Research Excellence Fund (CFREF).

7. Author contributions

JDX, TWS, JMT, MM conceptualized the work. MR designed the VWM task and collected and preprocessed the data. BC, RAG designed the CDM task and collected and preprocessed the data. RL designed the ODR task and collected and preprocessed the data. RAG performed surgical implantations. JMT contributed to experimental design. JDX analyzed the data and wrote the manuscript. MHM, LM, JD, MM provided analysis advice. JDX, TWS, JMT, MM edited the manuscript.

8. Declaration of interests

The authors declare no competing interests.

References

Arbuckle, S.A., Weiler, J., Kirk, E.A., Rice, C.L., Schieber, M., Pruszynski, J.A., Ejaz, N., Diedrichsen, J., 2020. Structure of Population Activity in Primary Motor Cortex for Single Finger Flexion and Extension. Journal of Neuroscience 40, 9210–9223. URL: https://www.jneurosci.org/content/40/48/9210, doi:10.1523/JNEUROSCI.0999-20.2020. publisher: Society for Neuroscience Section: Research Articles.

Bao, P., She, L., McGill, M., Tsao, D.Y., 2020. A map of object space in primate inferotemporal cortex. Nature 583, 103–108. URL: https://www.nature.com/articles/s41586-020-2350-5, doi:10.1038/s41586-020-2350-5. number: 7814 Publisher: Nature Publishing Group.

Bell, A.H., Hadj-Bouziane, F., Frihauf, J.B., Tootell, R.B.H., Ungerleider, L.G., 2009. Object Representations in the Temporal Cortex of Monkeys and Humans as Revealed by Functional Magnetic Resonance Imaging. Journal of Neurophysiology 101, 688–700. URL: https://www.ncbi.nlm.nih.gov/pmc/articles/PMC2657058/, doi:10.1152/jn.90657.2008.

Brewer, A.A., Press, W.A., Logothetis, N.K., Wandell, B.A., 2002. Visual areas in macaque cortex measured using functional magnetic resonance imaging. The Journal of Neuroscience: The Official Journal of the Society for Neuroscience 22, 10416–10426. doi:10.1523/JNEUROSCI.22-23-10416.2002.

Bugbee, N.M., Goldman-Rakic, P.S., 1983. Columnar organization of corticocortical projections in squirrel and rhesus monkeys: Similarity of column width in species differing in cortical volume. Journal of Comparative Neurology 220, 355–364. URL: https://onlinelibrary.wiley.com/doi/abs/10.1002/cne.902200309, doi:10.1002/cne.902200309. _eprint: https://onlinelibrary.wiley.com/doi/pdf/10.1002/cne.902200309.

Bullock, K.R., Pieper, F., Sachs, A.J., Martinez-Trujillo, J.C., 2017. Visual and presaccadic activity in area 8Ar of the macaque monkey lateral

prefrontal cortex. Journal of Neurophysiology 118, 15–28. URL: https://journals.physiology.org/doi/full/10.1152/jn.00278.2016, doi:10.1152/jn.00278.2016. publisher: American Physiological Society.

Cole, M.W., Bassett, D.S., Power, J.D., Braver, T.S., Petersen, S.E., 2014. Intrinsic and Task-Evoked Network Architectures of the Human Brain. Neuron 83, 238–251. URL: https://www.cell.com/article/S0896-6273(14)00400-0/fulltext, doi:10.1016/j.neuron.2014.05.014. publisher: Elsevier.

Cole, M.W., Ito, T., Bassett, D.S., Schultz, D.H., 2016. Activity flow over resting-state networks shapes cognitive task activations. Nature Neuroscience 19, 1718–1726. URL: https://www.nature.com/articles/nn.4406, doi:10.1038/nn.4406. number: 12 Publisher: Nature Publishing Group.

Corrigan, B.W., Gulli, R.A., Doucet, G., Roussy, M., Luna, R., Pradeepan, K.S., Sachs, A.J., Martinez-Trujillo, J.C., 2022. Distinct neural codes in primate hippocampus and lateral prefrontal cortex during associative learning in virtual environments. Neuron 110, 2155–2169.e4. URL: https://www.sciencedirect.com/science/article/pii/S0896627322003610, doi:10.1016/j.neuron.2022.04.016.

Cossell, L., Iacaruso, M.F., Muir, D.R., Houlton, R., Sader, E.N., Ko, H., Hofer, S.B., Mrsic-Flogel, T.D., 2015. Functional organization of excitatory synaptic strength in primary visual cortex. Nature 518, 399–403. URL: https://www.nature.com/articles/nature14182, doi:10.1038/nature14182. publisher: Nature Publishing Group.

Desimone, R., Duncan, J., 1995. Neural mechanisms of selective visual attention. Annual Review of Neuroscience 18, 193–222. doi:10.1146/annurev.ne.18.030195.001205.

Diedrichsen, J., Ridgway, G.R., Friston, K.J., Wiestler, T., 2011. Comparing the similarity and spatial structure of neural representations: A

pattern-component model. NeuroImage 55, 1665–1678. URL: https://www.sciencedirect.com/science/article/pii/S1053811911000796, doi:10.1016/j.neuroimage.2011.01.044.

Doucet, G., Gulli, R.A., Martinez-Trujillo, J.C., 2016. Cross-species 3D virtual reality toolbox for visual and cognitive experiments. Journal of Neuroscience Methods 266, 84–93. URL: https://www.sciencedirect.com/science/article/pii/S0165027016300152, doi:10.1016/j.jneumeth.2016.03.009.

Driscoll, L.N., Pettit, N.L., Minderer, M., Chettih, S.N., Harvey, C.D., 2017. Dynamic Reorganization of Neuronal Activity Patterns in Parietal Cortex. Cell 170, 986–999.e16. URL: https://www.cell.com/cell/abstract/S0092-8674(17)30828-0, doi:10.1016/j.cell.2017.07.021. publisher: Elsevier.

Duncan, J., 2001. An adaptive coding model of neural function in prefrontal cortex. Nature Reviews Neuroscience 2, 820–829. URL: https://www.nature.com/articles/35097575, doi:10.1038/35097575. number: 11 Publisher: Nature Publishing Group.

Duncan, J., Chylinski, D., Mitchell, D.J., Bhandari, A., 2017. Complexity and compositionality in fluid intelligence. Proceedings of the National Academy of Sciences 114, 5295–5299. URL: https://www.pnas.org/doi/full/10.1073/pnas.1621147114, doi:10.1073/pnas.1621147114. publisher: Proceedings of the National Academy of Sciences.

Fang, C., Cai, X., Lu, H.D., 2022. Orientation anisotropies in macaque visual areas. Proceedings of the National Academy of Sciences 119, e2113407119. URL: https://www.pnas.org/doi/full/10.1073/pnas.2113407119, doi:10.1073/pnas.2113407119. publisher: Proceedings of the National Academy of Sciences.

Freedman, D.J., Riesenhuber, M., Poggio, T., Miller, E.K., 2001. Categorical Representation of Visual Stimuli in the Primate Prefrontal Cortex. Science

291, 312–316. URL: https://www.science.org/doi/10.1126/science.291.5502.312, doi:10.1126/science.291.5502.312. publisher: American Association for the Advancement of Science.

Fusi, S., Miller, E.K., Rigotti, M., 2016. Why neurons mix: high dimensionality for higher cognition. Current Opinion in Neurobiology 37, 66–74. URL: https://www.sciencedirect.com/science/article/pii/S0959438816000118, doi:10.1016/j.conb.2016.01.010.

Fuster, J., 2015. The Prefrontal Cortex. Academic Press.

Goldman, P.S., Nauta, W.J.H., 1977. An intricately patterned prefronto-caudate projection in the rhesus monkey. Journal of Comparative Neurology 171, 369–385. URL: https://onlinelibrary.wiley.com/doi/abs/10.1002/cne.901710305, doi:10.1002/cne.901710305. _eprint: https://onlinelibrary.wiley.com/doi/pdf/10.1002/cne.901710305.

Goldman-Rakic, P.S., 1984. Modular organization of prefrontal cortex. Trends in Neurosciences 7, 419–424. URL: https://www.sciencedirect.com/science/article/pii/S0166223684801460, doi:10.1016/S0166-2236(84)80146-0.

Goldman-Rakic, P.S., 1988. Topography of Cognition: Parallel Distributed Networks in Primate Association Cortex. Annual Review of Neuroscience 11, 137–156. URL: https://doi.org/10.1146/annurev.ne.11.030188.001033, doi:10.1146/annurev.ne.11.030188.001033. _eprint: https://doi.org/10.1146/annurev.ne.11.030188.001033.

Goldman-Rakic, P.S., Schwartz, M.L., 1982. Interdigitation of Contralateral and Ipsilateral Columnar Projections to Frontal Association Cortex in Primates. Science 216, 755–757. URL: https://www.science.org/doi/10.1126/science.6177037, doi:10.1126/science.6177037. publisher: American Association for the Advancement of Science.

Gulli, R.A., Duong, L.R., Corrigan, B.W., Doucet, G., Williams, S., Fusi, S., Martinez-Trujillo, J.C., 2020. Context-dependent representations of objects and space in the primate hippocampus during virtual navigation. Nature Neuroscience 23, 103–112. URL: https://www.nature.com/articles/s41593-019-0548-3, doi:10.1038/s41593-019-0548-3. number: 1 Publisher: Nature Publishing Group.

Harel, A., Kravitz, D.J., Baker, C.I., 2014. Task context impacts visual object processing differentially across the cortex. Proceedings of the National Academy of Sciences 111, E962–E971. URL: https://www.pnas.org/doi/10.1073/pnas.1312567111, doi:10.1073/pnas.1312567111. publisher: Proceedings of the National Academy of Sciences.

Hubel, D.H., Wiesel, T.N., 1968. Receptive fields and functional architecture of monkey striate cortex. The Journal of Physiology 195, 215–243. doi:10.1113/jphysiol.1968.sp008455.

Ito, T., Murray, J.D., 2023. Multitask representations in the human cortex transform along a sensory-to-motor hierarchy. Nature Neuroscience 26, 306–315. URL: https://www.nature.com/articles/s41593-022-01224-0, doi:10.1038/s41593-022-01224-0. publisher: Nature Publishing Group.

Kiani, R., Cueva, C.J., Reppas, J.B., Peixoto, D., Ryu, S.I., Newsome, W.T., 2015. Natural Grouping of Neural Responses Reveals Spatially Segregated Clusters in Prearcuate Cortex. Neuron 85, 1359–1373. URL: https://www.sciencedirect.com/science/article/pii/S0896627315001282, doi:10.1016/j.neuron.2015.02.014.

King, M., Hernandez-Castillo, C.R., Poldrack, R.A., Ivry, R.B., Diedrichsen, J., 2019. Functional boundaries in the human cerebellum revealed by a multi-domain task battery. Nature Neuroscience 22, 1371–1378. URL: https://www.nature.com/articles/s41593-019-0436-x, doi:10.1038/s41593-019-0436-x. number: 8 Publisher: Nature Publishing Group.

Leavitt, M.L., Pieper, F., Sachs, A.J., Martinez-Trujillo, J.C., 2018. A Quadrantic Bias in Prefrontal Representation of Visual-Mnemonic Space. Cerebral Cortex 28, 2405–2421. URL: https://doi.org/10.1093/cercor/bhx142, doi:10.1093/cercor/bhx142.

Leichnetz, G.R., Spencer, R.F., Hardy, S.G.P., Astruc, J., 1981. The prefrontal corticotectal projection in the monkey; An anterograde and retrograde horseradish peroxidase study. Neuroscience 6, 1023–1041. URL: https://www.sciencedirect.com/science/article/pii/0306452281900683, doi:10.1016/0306-4522(81)90068-3.

Lennert, T., Cipriani, R., Jolicoeur, P., Cheyne, D., Martinez-Trujillo, J.C., 2011. Attentional Modulation of Neuromagnetic Evoked Responses in Early Human Visual Cortex and Parietal Lobe following a Rank-Order Rule. Journal of Neuroscience 31, 17622–17636. URL: https://www.jneurosci.org/content/31/48/17622, doi:10.1523/JNEUROSCI.4781-11.2011. publisher: Society for Neuroscience Section: Articles.

Lennert, T., Martinez-Trujillo, J.C., 2013. Prefrontal Neurons of Opposite Spatial Preference Display Distinct Target Selection Dynamics. The Journal of Neuroscience 33, 9520–9529. URL: https://www.jneurosci.org/lookup/doi/10.1523/JNEUROSCI.5156-12.2013, doi:10.1523/JNEUROSCI.5156-12.2013.

Luna, R., Roussy, M., Treue, S., Martinez-Trujillo, J.C., 2019. Reference Frames for Spatial Working Memory in the Lateral Prefrontal Cortex of primates. Journal of Vision 19, 206. URL: https://doi.org/10.1167/19.10.206, doi:10.1167/19.10.206.

Margolis, D.J., Lütcke, H., Schulz, K., Haiss, F., Weber, B., Kügler, S., Hasan, M.T., Helmchen, F., 2012. Reorganization of cortical population activity imaged throughout long-term sensory deprivation. Nature Neuroscience 15, 1539–1546. doi:10.1038/nn.3240.

Markowitz, D.A., Curtis, C.E., Pesaran, B., 2015. Multiple component networks support working memory in prefrontal cortex. Proceedings of the National Academy of Sciences 112, 11084–11089. URL: https://www.pnas.org/doi/10.1073/pnas.1504172112, doi:10.1073/pnas.1504172112. publisher: Proceedings of the National Academy of Sciences.

Masse, N.Y., Hodnefield, J.M., Freedman, D.J., 2017. Mnemonic Encoding and Cortical Organization in Parietal and Prefrontal Cortices. The Journal of Neuroscience 37, 6098–6112. URL: https://www.jneurosci.org/lookup/doi/10.1523/JNEUROSCI.3903-16.2017, doi:10.1523/JNEUROSCI.3903-16.2017.

McMahon, D.B.T., Bondar, I.V., Afuwape, O.A.T., Ide, D.C., Leopold, D.A., 2014. One month in the life of a neuron: longitudinal single-unit electrophysiology in the monkey visual system. Journal of Neurophysiology 112, 1748–1762. URL: https://journals.physiology.org/doi/full/10.1152/jn.00052.2014, doi:10.1152/jn.00052.2014. publisher: American Physiological Society.

Miller, E.K., Cohen, J.D., 2001. An Integrative Theory of Prefrontal Cortex Function. Annual Review of Neuroscience 24, 167–202. URL: https://doi.org/10.1146/annurev.neuro.24.1.167, doi:10.1146/annurev.neuro.24.1.167. _eprint: https://doi.org/10.1146/annurev.neuro.24.1.167.

Moran, P.A.P., 1950. Notes on Continuous Stochastic Phenomena. Biometrika 37, 17–23. URL: https://www.jstor.org/stable/2332142, doi:10.2307/2332142. publisher: [Oxford University Press, Biometrika Trust].

Muysers, H., Chen, H.L., Hahn, J., Folschweiller, S., Sigurdsson, T., Sauer, J.F., Bartos, M., 2024. A persistent prefrontal reference frame across time and task rules. Nature Communications 15, 2115. URL: https://www.nature.com/articles/s41467-024-46350-4, doi:10.1038/s41467-024-46350-4. publisher: Nature Publishing Group.

Rigotti, M., Barak, O., Warden, M.R., Wang, X.J., Daw, N.D., Miller, E.K., Fusi, S., 2013. The importance of mixed selectivity in complex cognitive tasks. Nature 497, 585–590. URL: https://www.nature.com/articles/nature12160, doi:10.1038/nature12160. number: 7451 Publisher: Nature Publishing Group.

Roussy, M., Luna, R., Duong, L., Corrigan, B., Gulli, R.A., Nogueira, R., Moreno-Bote, R., Sachs, A.J., Palaniyappan, L., Martinez-Trujillo, J.C., 2021. Ketamine disrupts naturalistic coding of working memory in primate lateral prefrontal cortex networks. Molecular Psychiatry 26, 6688–6703. URL: https://www.nature.com/articles/s41380-021-01082-5, doi:10.1038/s41380-021-01082-5. number: 11 Publisher: Nature Publishing Group.

Schmitz, T.W., Duncan, J., 2018. Normalization and the Cholinergic Microcircuit: A Unified Basis for Attention. Trends in Cognitive Sciences 22, 422–437. URL: https://www.sciencedirect.com/science/article/pii/S1364661318300470, doi:10.1016/j.tics.2018.02.011.

Tanaka, K., 1996. Inferotemporal cortex and object vision. Annual Review of Neuroscience 19, 109–139. doi:10.1146/annurev.ne.19.030196.000545.

Vul, E., Harris, C., Winkielman, P., Pashler, H., 2009. Puzzlingly High Correlations in fMRI Studies of Emotion, Personality, and Social Cognition. Perspectives on Psychological Science 4, 274–290. URL: https://doi.org/10.1111/j.1745-6924.2009.01125.x, doi:10.1111/j.1745-6924.2009.01125.x. publisher: SAGE Publications Inc.

Wandell, B.A., Dumoulin, S.O., Brewer, A.A., 2007. Visual Field Maps in Human Cortex. Neuron 56, 366–383. URL: https://www.sciencedirect.com/science/article/pii/S089662730700774X, doi:10.1016/j.neuron.2007.10.012.

Xu, R., Bichot, N.P., Takahashi, A., Desimone, R., 2022. The cortical connectome of primate lateral prefrontal cortex. Neuron 110, 312–

327.e7. URL: https://www.sciencedirect.com/science/article/pii/S0896627321007868, doi:10.1016/j.neuron.2021.10.018.

Xu, T., Nenning, K.H., Schwartz, E., Hong, S.J., Vogelstein, J.T., Goulas, A., Fair, D.A., Schroeder, C.E., Margulies, D.S., Smallwood, J., Milham, M.P., Langs, G., 2020. Cross-species functional alignment reveals evolutionary hierarchy within the connectome. NeuroImage 223, 117346. URL: https://www.sciencedirect.com/science/article/pii/S1053811920308326, doi:10.1016/j.neuroimage.2020.117346.

Yacoub, E., Harel, N., Uğurbil, K., 2008. High-field fMRI unveils orientation columns in humans. Proceedings of the National Academy of Sciences 105, 10607–10612. URL: https://www.pnas.org/doi/10.1073/pnas.0804110105, doi:10.1073/pnas.0804110105. publisher: Proceedings of the National Academy of Sciences.

Yang, G.R., Cole, M.W., Rajan, K., 2019a. How to study the neural mechanisms of multiple tasks. Current Opinion in Behavioral Sciences 29, 134–143. URL: https://www.sciencedirect.com/science/article/pii/S2352154619300695, doi:10.1016/j.cobeha.2019.07.001.

Yang, G.R., Joglekar, M.R., Song, H.F., Newsome, W.T., Wang, X.J., 2019b. Task representations in neural networks trained to perform many cognitive tasks. Nature Neuroscience 22, 297–306. URL: https://www.nature.com/articles/s41593-018-0310-2, doi:10.1038/s41593-018-0310-2. number: 2 Publisher: Nature Publishing Group.

Yu, B.M., Cunningham, J.P., Santhanam, G., Ryu, S.I., Shenoy, K.V., Sahani, M., 2009. Gaussian-Process Factor Analysis for Low-Dimensional Single-Trial Analysis of Neural Population Activity. Journal of Neurophysiology 102, 614–635. URL: https://journals.physiology.org/doi/full/10.1152/jn.90941.2008, doi:10.1152/jn.90941.2008. publisher: American Physiological Society.